significance among data sets. These tests were implemented within GraphPad Prism software (GraphPad Software). Significance was defined as $p<0.05$.

RESULTS

Aβ oligomerization - To determine whether the five phenolic compounds blocked formation of low n-order Aβ oligomers, we used PICUP, a photochemical cross-linking method that is rapid, efficient, requires no structural modification of Aβ, and accurately reveals the oligomerization state of Aβ (21). In the absence of cross-linking, only Aβ40 monomers (**Fig. 2A**) and Aβ42 monomers and trimers (**Fig. 2B**) were observed. The Aβ42 trimer band has been shown to be an SDS-induced artifact (21). Following cross-linking, and as reported previously (21), Aβ40 existed predominately as a mixture of monomers and oligomers of order 2-4 (**Fig. 2A**,) whereas Aβ42 comprised predominately monomers and oligomers of order 2-6 (**Fig. 2B**).

When 10 μM Myr was mixed with Aβ40 at a peptide:compound ratio of 5:2, oligomerization was blocked slightly (**Fig. 2A**). The intensity of tetramer band was decreased. When 100 μM Myr was mixed with Aβ40 at a peptide:compound ratio of 1:4, oligomerization was blocked almost completely (**Fig. 2A**). The effect of Myr on Aβ42 oligomerization was equally significant (**Fig. 2B**). When 10 μM Myr was mixed with Aβ42 at a peptide:compound ratio of 5:2, oligomerization was blocked moderately. The pentamer and hexamer bands disappeared, and the intensity of tetramer band markedly decreased (**Fig. 2B**). At peptide:compound ratio of 1:4, Myr produced oligomer distributions almost identical to those of untreated Aβ42, consistent with an essentially complete inhibition of oligomerization (**Fig. 2B**). When 10 or 100 μM RA was mixed with Aβ40 or Aβ42 at the same ratios as used above, comparable effects were observed on Aβ oligomerization (**Figs. 2A and B**).

With Aβ40:FA at a 5:2 ratio, no inhibition of oligomerization was observed (**Fig. 2A**). At a higher concentration of FA (Aβ40:FA, 1:4), the trimer and tetramer bands disappeared, and the intensity of dimer band decreased (**Fig. 2A**). Similarly, with Aβ42:FA at a 5:2 ratio, no inhibition of the oligomerization was observed (**Fig. 2B**), while at higher concentration of FA (Aβ42:FA, 1:4), the pentamer and hexamer bands disappeared, and the intensity of tetramer band weakened (**Fig. 2B**).

When 10 or 100 μM NDGA was mixed with Aβ40 or Aβ42, similar strong effects was observed on Aβ oligomerization (**Figs. 2A and B**).

When 10 μM Cur was mixed with Aβ40 at a peptide:compound ratio of 5:2, no inhibition of oligomerization was observed (**Fig. 2A**). When 100 μM Cur was mixed with Aβ40 at a peptide:compound ratio of 1:4, oligomerization was blocked slightly (**Fig. 2A**). The intensity of tetramer band was decreased slightly. Similarly, when 10 μM Cur was mixed with Aβ42 at a peptide:compound ratio of 5:2, no inhibition of oligomerization was observed (**Fig. 2B**). At higher concentration of Cur (Aβ42:Cur, 1:4), oligomerization was blocked slightly (**Fig. 2B**). The intensities of dimer, pentamer, and hexamer band were decreased slightly.

We confirmed dose-dependency of these inhibitions (**Fig. S2**). The effective concentrations (EC_{50}) of Myr, FA, NDGA, Cur, and RA for the Aβ40 oligomerization were 12.4, 76.2, 34.5, 60.8, and 25.6 μM, respectively. The effective concentrations (EC_{50}) of Myr, FA, NDGA, Cur, and RA for the Aβ42 oligomerization were 7.0, 52.6, 38.3, 108.2, and 10.8 μM, respectively. Taken together, the data indicate that inhibitory activity of Aβ40 and Aβ42 oligomerization by the phenolic compounds examined in this study may be in the following order: Myr > RA > NDGA = FA ≥ Cur.

In the absence of cross-linking, only $[Met(O)^{35}]$Aβ42 monomers were observed (**Fig. S3**). Following cross-linking, and as reported previously (29), $[Met(O)^{35}]$Aβ42 existed predominately as a mixture of monomers and oligomers of order 2-5 (**Fig. S3**). When 10 or 100 μM Myr was mixed with $[Met(O)^{35}]$Aβ42, oligomerization was blocked significantly (**Fig. S3**). The intensity of trimer, tetramer and pentamer bands disappeared, and the intensity of dimer band markedly decreased. Similar effects were observed when 10 or 100 μM RA was mixed with $[Met(O)^{35}]$Aβ42 (**Fig. S3**).

A potential problem relates to the possibility that the strong inhibition of Aβ oligomerization could have resulted from an alternative compound, which may form from a possible side-reaction of the inhibitor and the PICUP sensitizer. To evaluate this possibility, cross-linking reactions also were performed on glutathione-S-transferase (GST; ~26 kDa), a positive control for the cross-linking chemistry (30). Uncross-linked GST exhibited an intense monomer band and a relatively faint dimer band (**Fig. 2C**). Cross-linking produced an intense dimer band, expected because GST exists normally as a homodimer, as well as higher-order cross-linked species. No alterations in GST cross-linking were observed in the presence of Myr, FA, NDGA, Cur, or RA at either of the two protein:compound ratios tested, 5:2 or 1:4 (**Fig. 2C**). Thus, the significant inhibition of Aβ40 and Aβ42 oligomerization is from a direct interaction with the phenolic compounds.

Aβ assembly morphology - To determine the morphology of the small assemblies present following PICUP of Aβ40 and Aβ42 with or without phenolic compounds, we used AFM. The height of uncross-linked Aβ40 was 0.23 ± 0.03 nm (**Fig. 2D** and **Table S1**). Following PICUP, the height of Aβ40 oligomers became 0.90 ± 0.05 nm (**Fig. 2F** and **Table S1**). The height of uncross-linked Aβ42 was 0.33 ± 0.02 nm (**Fig. 2E** and **Table S1**). Following PICUP, the height of Aβ42 oligomers became 1.39 ± 0.09 nm (**Fig. 2G** and **Table S1**). These morphologies are not inconsistent with our previous findings (7,22). When Aβ40 was cross-linked with Myr at a compound:peptide ratio of 4:1, the height of treated Aβ40 decreased to 0.32 ± 0.03 nm (**Fig. 2H** and **Table S1**). When Aβ40 was cross-linked with RA at a compound:peptide ratio of 4:1, the height of treated Aβ40 decreased to 0.42 ± 0.04 nm (**Fig. 2J** and **Table S1**). Similarly, when Aβ42 was cross-linked with Myr or RA at a compound:peptide ratio of 4:1, the height of treated Aβ40 decreased clearly (**Figs. 2I, 2K** and **Table S1**).

Aβ secondary structure dynamics - The above oligomerization studies revealed effects of the phenolic compounds at the initial stages of peptide self-association. To examine whether the phenolic compounds altered the secondary structure of the Aβ, we undertook CD studies (**Fig. 3**). Aβ40 and Aβ42, incubated alone, produced initial spectra characteristic of statistical coils (SC) (**Figs. 3A and B**). The major feature of these spectra was a large magnitude minimum centered at ~198 nm. Aβ40 displayed substantial secondary structure changes between days 3-5 that were consistent with previously reported SC→α-helix/β-sheet→β-sheet transitions associated with monomer→protofibril→fibril assembly (19). The Aβ42 system displayed similar structural changes, although, as expected, these changes occurred at much faster rate (0-2 days). When Aβ40 or Aβ42 were incubated with Myr at a compound:peptide ratio of 4:1, no such transitions were observed (**Figs. 3C and D**). Similarly, no such transitions were observed in the presence of RA (**Figs. 3E and F**). All spectra of Aβ40 and Aβ42 treated by Myr or RA revealed populations of conformers that were largely statistical coil.

NMR studies - The binding between the phenolic compounds and the Aβ42 was explored using NMR spectroscopy, a well-accepted tool for obtaining atomic level aspects of protein structure and ligand binding. The sample preparation protocol and lower NMR probe temperature (5°C) ensured that the Aβ42 remained monomeric during the entire data acquisition period (20,31). Standard heteronuclear single quantum coherence (HSQC) spectra were obtained with uniformly ^{15}N-labeled Aβ42, and the compound:peptide was kept at a 20:1 molar ratio. The HSQC experiment detects ^{1}H signals that are directly bonded to the ^{15}N atoms, and thus provides a fingerprint of the amide-NH backbone atoms. In the present study, the HSQC data demonstrate that the phenolic compounds do not induce AβMet35^{red} → AβMet35^{ox} oxidation (20).

Shown in **Fig. 4** are superimposed HSQC spectra of the Aβ42 alone (black crosspeaks) and the Aβ42 containing RA (**Fig. 4A**, red crosspeaks) and Myr (**Fig. 4B**, red crosspeaks). Because the cross peaks of the superimposed

spectra in **Fig. 4A** coincide, this indicates that RA does not bind with monomeric Aβ42. By contrast, the HSQC spectra with Myr show pronounced NH chemical shift movements (labeled peaks in **Fig. 4B**) indicative of binding. The most pronounced movements (0.02-0.05 ppm) were in the ^{1}H dimension and were among the R5, V12, H13, K16, L17, V18, F19, F20, A21, E23, D23, I31, and I32 residues. Besides movements, NH peak broadening occurred with R5, V12, K16, and V18, suggesting that the binding may be stronger with these residues. Less peak movements were seen with FA, NDGA, and Cur, and were not localized to any specific peptide region (**Fig. S4**).

The binding of RA and Myr were further explored using STD experiments, which is a well-established homonuclear NMR technique that permits detection of transient binding of small molecule ligands to macromolecular receptors. Notably, the STD has been used to discriminate ligand binding to monomeric or oligomeric states of the Aβ that co-exist in solution (23,32,33). In the STD, two separate spectra are obtained and then subtracted, where one spectra involves saturation of a resonance that belongs to the receptor (in this case the Aβ), while the second spectra involves saturation in a far-removed region that does not contain signals. The presence and strength of signals in the STD is indicative of binding.

Shown in **Fig. S5** are three groups of spectral data: Aβ40 alone (**Figs. S5A and B**), Aβ40 with RA (**Figs. S5C and D**), and Aβ40 with Myr (**Figs. S5E and F**). As expected, the STD spectra of Aβ40 alone (**Fig. S5B**) has no signals. By contrast, spectra containing RA (**Fig. S5D**) has extremely weak, barely-discernable peaks while that containing Myr (**Fig. S5F**) has obvious peaks. Because solution NMR detects only monomeric Aβ (20,23), these data demonstrate that Myr binds to monomeric Aβ while RA does not bind or binds very weakly. Overall, these results are consistent with the above HSQC data.

Highlighted in **Fig. 5** are molecular models of the Aβ42 that were obtained from a combined molecular dynamics and NMR approach (26). In solution, the Aβ42 adopts a rapidly equilibrating ensemble of conformations, which, for the monomeric aggregation state are predominately unstructured (20,31). These models effectively depict a single, highly-populated conformation that has β-hairpin at residues I31-L34 and G37-I41. The regions showing phenol-induced chemical shifts are colored in red, and because RA did not promote changes (**Fig. 4A**), only the green unlabeled backbone structure is shown. It is obvious that Myr causes extensive changes throughout the sequence, with continuous 9- and 3-residue spans at K16-V24 and I31-G33. By contrast, FA, NDGA, and Cur interactions are more limited, and interestingly occur at identical residues: R5, S8, G9, H133, K16, D23, and I31 (Cur also causes shifts of L17). With the exception of RA, all phenolic compounds have a proclivity for polar or charged amino acid residues.

Cellular toxicity - The ability of Myr and RA to inhibit formation of low-n Aβ oligomers suggested that it might be useful in blocking the Aβ-mediated cellular toxicity. To address this possibility, we performed MTT assays (34) and probed the cellular metabolism of human embryonic kidney (HEK) 293 cells. The MTT assay constitutes a rapid and sensitive method for determination of gross Aβ toxicity in cultures of dissociated cells (35).

Previous short duration incubation experiments established that the cross-linked Aβ40 and Aβ42 oligomers were more toxic than uncross-linked oligomers (7,22). In the present study, we explored the immediate consequences (i.e., no incubation time) on the viability of cells. Overall, the results are consistent with the previous study, in that uncross-linked and cross-linked Aβ42 oligomers (1 μM concentration and added immediately to the cells) showed cell viabilities of ~95% and ~79%, respectively. Thus, the cross-linked oligomers were significantly more toxic than uncross-linked oligomers ($p < 0.05$) (**Fig. S6**). Repeating the experiments with Myr showed almost a complete loss of cell toxicity, with the cross-linked oligomer with Myr producing slightly lower toxicity ($p < 0.05$). Using RA (instead of Myr) also reduced the toxicity to ≈ 6%, which was a major reduction relative to cross-linked Aβ42 ($p < 0.05$).

Similar observations were made in experiments with Aβ42 at higher concentrations

(10 μM) (**Fig. S6**). Uncross-linked and cross-linked Aβ42 displayed ~53% and ~44% cell viability levels, respectively, revealing a trend towards higher toxicity with cross-linked Aβ42. Myr and RA treatment increased cell viability significantly, 69% and 64% ($p < 0.01$) higher, respectively. In summary, regardless of the cross-linked state, Myr and RA are effective in disrupting the cellular toxicity associated with low-n Aβ42 oligomers.

Electrophysiology - To obtain an index of Aβ42-induced functional alteration of synaptic transmission, we analyzed LTP and LTD in the CA1 region of mouse hippocampal slices. Synaptic current strength was estimated from field excitatory postsynaptic potentials (fEPSP) slope (**Figs. 6A and B**). The vehicle group indicated LTP by tetanus stimulation (150 ± 6.7%). Cross-linked Aβ42 completely inhibited induction of LTP (97.5 ± 7.6%) without any alterations in baseline transmission. In contrast, cross-linked Aβ42 treated with Myr and RA induced LTP comparable to that of the vehicle alone (157 ± 5.1% and 144 ± 11.1%, respectively). Uncross-linked Aβ42 also induced LTP comparable to that in the vehicle (140 ± 10.1%). **Fig. 6C** shows differences in LTP induction among the five treatment groups. There was a significant group effect on %fEPSP slope [$F(4,22) = 6.295$, $p < 0.005$]. The post-hoc tests showed that %fEPSPs slope in the cross-linked Aβ42 group was significantly lower than those in the other four groups (**Fig. 6C**, $^{**}p<0.01$), indicating that cross-linked Aβ42 induced LTP suppression, but cross-linked Aβ42 treated with Myr and RA did not.

Low frequency conditioning stimulation (1 Hz, 450 paired-pulse) induced a transient decrease in %fEPSP slope beyond the 95% lower confidence limit of the baselines in all groups (**Figs. 6D and E**). This short-term decrease in synaptic transmission gradually recovered, and the vehicle group showed %fEPSP slope comparable to the baseline level (104.2 ± 10.1%) during 50-60 min after LTD induction. The cross-linked Aβ42 with Myr and RA as well as uncross-linked Aβ42 groups also showed %fEPSP slopes comparable to the baseline level (102 ± 2.6, 94 ± 4.2, and 105 ± 9.4%, respectively) during 50-60 min after LTD induction. However, the cross-linked Aβ42 group showed LTD (69 ± 6.6%) by low frequency conditioning stimulation. **Fig. 6F** shows differences in LTD induction among the five treatment groups. There was a significant group effect on %fEPSP slopes [$F(4,20) = 6.925$, $p < 0.005$]. The post-hoc tests showed that fEPSP in the cross-linked Aβ42 group was significantly lower than that in the other four groups (**Fig. 6F**, $^{*}p < 0.05$, $^{**}p < 0.01$), indicating that cross-linked Aβ42 induced LTD facilitation, but not cross-linked Aβ42 treated with Myr and RA.

DISCUSSION

We previously reported that phenolic compounds are effective *in vitro* inhibitors of fAβ formation and could destabilize preformed fAβ (14-16). Our subsequent *in vivo* work with Tg2576 mice established that Myr and RA reduced the amount of Aβ oligomers in the brain and prevented the development of AD pathology (18). The purpose of the present study was to unravel chemical and neurophysiological bases for these effects, which could accelerate the development of more effective aggregation inhibitors.

Fig. S7 presents a summary of how the polyphenols interfere with Aβ aggregation. The monomer → soluble oligomer → soluble β-sheet oligomer → protofibril → mature fibril is generally recognized as the normal "on-pathway" process associated with plaque formation of the Aβ and other amyloid forming proteins. The PICUP studies revealed that all five phenolic compounds dose-dependently inhibited Aβ40 and Aβ42 later-stage oligomerization, and the PICUP method requires that monomers be in close proximity for covalent cross-linking to occur. The CD studies showed that Myr and RA stabilized Aβ populations comprising mostly random coil and inhibited SC → β-sheet conversion, which was consistent with the PICUP data. However, at the atomic level, NMR showed that Myr and RA behave differently, in that Myr shows significant binding to monomeric Aβ42, whereas RA does not bind to the monomer. This result is

intriguing, in that it is possible that RA could prevent aggregation by binding with non-NMR detectable early-formed oligomers (dimers, trimers, etc.)(36), and in doing so prevents neurotoxicity by binding to an exposed toxic structural motif. Other Aβ binding compounds bind in a similar manner, including human serum albumin (32), apolipoprotein E3 (37), and alcohol dehydrogenase (38). Another possibility is that RA may bind to distinct monomer conformers/structures that in turn inhibit oligomerization (39).

The NMR studies also established that Myr, NDGA, FA, and Cur bind to localized or specific monomeric Aβ peptide regions (**Fig. 5**), which are R5, S8, G9, H13, K16, D23, and I31. The polyphenol (-)-epigallocatechin gallate prevents α-synuclein (αS) (40) and Aβ42 aggregation by also binding to small (localized) amino acid regions. Related work (41) reported that the flavonoid baicalein stabilized a partially folded conformer of αS that existed within oligomeric assemblies. Conway *et al.* (42) showed that dopamine or levodopa inhibits the fibrillization of αS filaments, presumably through stabilization of αS into protofibrillar structures unable to form fibrils. Taniguchi *et al.* (43) reported the formation of tau oligomers in the presence of phenothiazines, polyphenols, or porphyrins. In each of these cases, the inhibitors stabilized oligomeric states, in which the respective protein maintained at least a partial fold. For Aβ, if the "oligomer cascade" hypothesis is true, (2) aggregation inhibitors that stabilize oligomers could produce peptide populations of enhanced toxicity. The observation that some of the phenolic compounds bind monomeric Aβ and prevent its oligomerization is a particularly important feature.

Because our NMR study does not show strong interactions between the phenolic compounds and the Aβ, it is possible that other mechanisms may be operative, particularly with the in vivo animal studies (18). Leong *et al.* (44) reported that dopamine could oxidize methionine of αS peptide, and in the process alter the aggregation properties of the protein. We previously reported that [Met(O)^{35}]Aβ42 demonstrated different oligomer distributions than wild type Aβ42 with reduced Met35 (29). In our study, both Myr and RA inhibited [Met(O)^{35}]Aβ42 oligomerization similarly with wild type Aβ42 oligomerization. However, because the HSQC data established that the phenolic compounds did not induce AβMet35^{red} → AβMet35^{ox} oxidation, Myr and RA may inhibit Aβ oligomerization without regard to oxidative modification.

With our previous Tg2576 mice study (18), RA was very promising because it inhibited both HMW Aβ oligomerization and Aβ deposition, while FA did not inhibit either process. However, our present *in vitro* studies demonstrate that all phenolic compounds (including FA) prevent low order (< 10 monomers) oligomer formation. This discrepancy could be due to the non-specific nature of the A11 antibody that was used to detect oligomers in the Tg2576 mice (18), particularly when compared to cross-linked oligomers detected by the PICUP. Similar findings were reported by Necula *et al.*, (45) where dot blot assays with the A11 antibody showed that Myr, NDGA, and Cur inhibited HMW Aβ oligomerization but not fibrillization.

Myr and RA decreased Aβ oligomer-induced synaptic toxicities using LTP and LTD assays of hippocampal slices. LTP and LTD are considered important neurophysiological models of memory and learning and are used as experimental models of neuronal plasticity (46). Townsend *et al.* found that Aβ trimers fully inhibit LTP, whereas dimers and tetramers have an intermediate potency (4). Dimers and trimers from the conditioned medium of APP-expressing CHO cells have been found to cause progressive loss of synapses in organotypic rat hippocampal slices (5). Aβ oligomers extracted from AD brains potently inhibited LTP and enhanced LTD, indicating disruption of synapse structure and function (6). Our studies are consistent with the previous studies(4-6), where Aβ oligomers suppressed LTP and facilitated LTD induction. Both suppression of LTP and facilitation of LTD induction in the hippocampal CA1 subfield suggests that memory formation is disturbed by Aβ oligomers. In contrast, Aβ monomers resulting from reaction with phenolic compounds did not induce such effects. These

findings suggest that phenolic compounds have preventive effects on Aβ-induced memory deficits. Recent studies suggested that Aβ-induced inhibition of LTP was due to a decrease in density of the NR2B subunit of NMDA receptor at the postsynaptic membrane, and facilitation of LTD was ascribed to an increase in glutamate concentration at the synaptic cleft (47,48). These studies suggest that Aβ toxicity could selectively affect these synaptic functions with usual cell functions relatively intact in brief exposure. Therefore, deficits in Aβ-induced neuronal plasticity observed in the present study might be related to early neurophysiological alterations prior to histopathological changes such as neuronal loss and brain atrophy in AD.

Myr is found in various foods, including onions, berries, and grapes, as well as red wine (49). Many studies indicate that Myr has various biological activities, such as antioxidant, anti-inflammatory, anticarcinogen, and antiviral (49). Recently, Myr was reported to act as a β-secretase inhibitor with reduced production of Aβ in a cell culture study (50). FA is a major constituent of fruits and is well-known to be an important antioxidant (51). Long-term administration of FA was reported to protect mice against Aβ-induced learning and memory deficits *in vivo* (52), and FA protects neurons against Aβ-induced oxidative stress and neurotoxicity *in vitro* (53). NDGA is a pure compound isolated from the creosote bush, *Larrea tridentate* (54). NDGA also suppresses Aβ-induced accumulation of reactive oxygen species (55). Cur is a potent antioxidant and an effective anti-inflammatory compound (56). Several studies suggested that Cur could be a key molecule for the development of therapeutics for AD (57-59). Cur protected PC12 and human umbilical vein endothelial cells from Aβ insult due to its strong antioxidant properties (58), and dietary curcumin prevented Aβ-infusion induced spatial memory deficits and reduced Aβ deposits in rats (59). RA is an ester of caffeic acid and 3,4-dihydroxiphenyllactic acid. It is commonly found in species of the *Boraginaceae* and subfamily *Nepetoideae* of the *Lamiaceae* (60). It has several interesting biological activities, e.g., antioxidant, anti-inflammatory, antimutagen, antibacterial, and antiviral (60). For the anti-Aβ effect, there have been reports that RA reduces Aβ-induced neurotoxicity (61,62).

In conclusion, our results established that the phenolic compounds inhibit the oligomerization and the SC → β-sheet conversion of Aβ40 and Aβ42, while NMR revealed phenolic compound binding sites. In addition, the MTT, LTP and LTD assays established that the phenols inhibit Aβ oligomer-induced cellular and synaptic toxicites. These data, coupled with previously reported antioxidant and ameliorative effects, suggest that phenolic compounds are worthy therapeutic candidates for AD.

REFERENCES

1. Haass, C., and Selkoe, D. J. (2007) *Nat Rev Mol Cell Biol* **8**, 101-112
2. Roychaudhuri, R., Yang, M., Hoshi, M. M., and Teplow, D. B. (2009) *J Biol Chem* **284**, 4749-4753
3. Ono, K., and Yamada, M. (2011) *J Neurochem* **117**, 19-28
4. Townsend, M., Shankar, G. M., Mehta, T., Walsh, D. M., and Selkoe, D. J. (2006) *J Physiol* **572**, 477-492
5. Shankar, G. M., Bloodgood, B. L., Townsend, M., Walsh, D. M., Selkoe, D. J., and Sabatini, B. L. (2007) *J Neurosci* **27**, 2866-2875
6. Shankar, G. M., Li, S., Mehta, T. H., Garcia-Munoz, A., Shepardson, N. E., Smith, I., Brett, F. M., Farrell, M. A., Rowan, M. J., Lemere, C. A., Regan, C. M., Walsh, D. M., Sabatini, B. L., and Selkoe, D. J. (2008) *Nat Med* **14**, 837-842
7. Ono, K., Condron, M. M., and Teplow, D. B. (2009) *Proc Natl Acad Sci U S A* **106**, 14745-14750

8. Orgogozo, J. M., Dartigues, J. F., Lafont, S., Letenneur, L., Commenges, D., Salamon, R., Renaud, S., and Breteler, M. B. (1997) *Rev Neurol (Paris)* **153**, 185-192
9. Truelsen, T., Thudium, D., and Gronbaek, M. (2002) *Neurology* **59**, 1313-1319
10. Flamini, R. (2003) *Mass Spectrom Rev* **22**, 218-250
11. Marambaud, P., Zhao, H., and Davies, P. (2005) *J Biol Chem* **280**, 37377-37382
12. Sharma, R. A., Gescher, A. J., and Steward, W. P. (2005) *Eur J Cancer* **41**, 1955-1968
13. Ganguli, M., Chandra, V., Kamboh, M. I., Johnston, J. M., Dodge, H. H., Thelma, B. K., Juyal, R. C., Pandav, R., Belle, S. H., and DeKosky, S. T. (2000) *Arch Neurol* **57**, 824-830
14. Ono, K., Yoshiike, Y., Takashima, A., Hasegawa, K., Naiki, H., and Yamada, M. (2003) *J Neurochem* **87**, 172-181
15. Ono, K., Hasegawa, K., Naiki, H., and Yamada, M. (2004) *J Neurosci Res* **75**, 742-750
16. Ono, K., Hirohata, M., and Yamada, M. (2005) *Biochem Biophys Res Commun* **336**, 444-449
17. Wang, J., Ho, L., Zhao, W., Ono, K., Rosensweig, C., Chen, L., Humala, N., Teplow, D. B., and Pasinetti, G. M. (2008) *J Neurosci* **28**, 6388-6392
18. Hamaguchi, T., Ono, K., Murase, A., and Yamada, M. (2009) *Am J Pathol* **175**, 2557-2565
19. Ono, K., Condron, M. M., Ho, L., Wang, J., Zhao, W., Pasinetti, G. M., and Teplow, D. B. (2008) *J Biol Chem* **283**, 32176-32187
20. Hou, L., Shao, H., Zhang, Y., Li, H., Menon, N. K., Neuhaus, E. B., Brewer, J. M., Byeon, I. J., Ray, D. G., Vitek, M. P., Iwashita, T., Makula, R. A., Przybyla, A. B., and Zagorski, M. G. (2004) *J Am Chem Soc* **126**, 1992-2005
21. Bitan, G., and Teplow, D. B. (2004) *Acc Chem Res* **37**, 357-364
22. Ono, K., Condron, M. M., and Teplow, D. B. (2010) *J Biol Chem* **285**, 23186-23197
23. Narayanan, S., and Reif, B. (2005) *Biochemistry* **44**, 1444-1452
24. Milojevic, J., Esposito, V., Das, R., and Melacini, G. (2007) *J Am Chem Soc* **129**, 4282-4290
25. Delaglio, F., Grzesiek, S., Vuister, G. W., Zhu, G., Pfeifer, J., and Bax, A. (1995) *J Biomol NMR* **6**, 277-293
26. Sgourakis, N. G., Yan, Y., McCallum, S. A., Wang, C., and Garcia, A. E. (2007) *Journal of Molecular Biology* **368**, 1448-1457
27. Guex, N., and Peitsch, M. C. (1997) *Electrophoresis* **18**, 2714-2723
28. Soeda, Y., Tsuneki, H., Muranaka, H., Mori, N., Hosoh, S., Ichihara, Y., Kagawa, S., Wang, X., Toyooka, N., Takamura, Y., Uwano, T., Nishijo, H., Wada, T., and Sasaoka, T. (2010) *Mol Endocrinol* **24**, 1965-1977
29. Bitan, G., Tarus, B., Vollers, S. S., Lashuel, H. A., Condron, M. M., Straub, J. E., and Teplow, D. B. (2003) *J Am Chem Soc* **125**, 15359-15365
30. Fancy, D. A., and Kodadek, T. (1999) *Proc Natl Acad Sci U S A* **96**, 6020-6024
31. Yan, Y., and Wang, C. (2006) *J Mol Biol* **364**, 853-862
32. Milojevic, J., Raditsis, A., and Melacini, G. (2009) *Biophys J* **97**, 2585-2594
33. Huang, H., Milojevic, J., and Melacini, G. (2008) *J Phys Chem B* **112**, 5795-5802
34. Abe, K., and Saito, H. (1998) *Neurosci Res* **31**, 295-305
35. Ronicke, R., Klemm, A., Meinhardt, J., Schroder, U. H., Fandrich, M., and Reymann, K. G. (2008) *PLoS One* **3**, e3236
36. Fawzi, N. L., Ying, J., Torchia, D. A., and Clore, G. M. (2010) *J Am Chem Soc* **132**, 9948-9951
37. Evans, K. C., Berger, E. P., Cho, C. G., Weisgraber, K. H., and Lansbury, P. T., Jr. (1995) *Proc Natl Acad Sci U S A* **92**, 763-767
38. Yan, Y., Liu, Y., Sorci, M., Belfort, G., Lustbader, J. W., Yan, S. S., and Wang, C. (2007) *Biochemistry* **46**, 1724-1731
39. Rojas, A., Liwo, A., Browne, D., and Scheraga, H. A. (2010) *J Mol Biol* **404**, 537-552
40. Ehrnhoefer, D. E., Bieschke, J., Boeddrich, A., Herbst, M., Masino, L., Lurz, R., Engemann, S., Pastore, A., and Wanker, E. E. (2008) *Nat Struct Mol Biol* **15**, 558-566
41. Zhu, M., Rajamani, S., Kaylor, J., Han, S., Zhou, F., and Fink, A. L. (2004) *J Biol Chem* **279**, 26846-26857
42. Conway, K. A., Rochet, J. C., Bieganski, R. M., and Lansbury, P. T., Jr. (2001) *Science* **294**, 1346-1349
43. Taniguchi, S., Suzuki, N., Masuda, M., Hisanaga, S., Iwatsubo, T., Goedert, M., and Hasegawa,

M. (2005) *J Biol Chem* **280**, 7614-7623
44. Leong, S. L., Pham, C. L., Galatis, D., Fodero-Tavoletti, M. T., Perez, K., Hill, A. F., Masters, C. L., Ali, F. E., Barnham, K. J., and Cappai, R. (2009) *Free Radic Biol Med* **46**, 1328-1337
45. Necula, M., Kayed, R., Milton, S., and Glabe, C. G. (2007) *J Biol Chem* **282**, 10311-10324
46. Martin, S. J., Grimwood, P. D., and Morris, R. G. (2000) *Annu Rev Neurosci* **23**, 649-711
47. Snyder, E. M., Nong, Y., Almeida, C. G., Paul, S., Moran, T., Choi, E. Y., Nairn, A. C., Salter, M. W., Lombroso, P. J., Gouras, G. K., and Greengard, P. (2005) *Nat Neurosci* **8**, 1051-1058
48. Li, S., Hong, S., Shepardson, N. E., Walsh, D. M., Shankar, G. M., and Selkoe, D. (2009) *Neuron* **62**, 788-801
49. Ong, K. C., and Khoo, H. E. (1997) *Gen Pharmacol* **29**, 121-126
50. Shimmyo, Y., Kihara, T., Akaike, A., Niidome, T., and Sugimoto, H. (2008) *Biochim Biophys Acta* **1780**, 819-825
51. Scott, B. C., Butler, J., Halliwell, B., and Aruoma, O. I. (1993) *Free Radic Res Commun* **19**, 241-253
52. Yan, J. J., Cho, J. Y., Kim, H. S., Kim, K. L., Jung, J. S., Huh, S. O., Suh, H. W., Kim, Y. H., and Song, D. K. (2001) *Br J Pharmacol* **133**, 89-96
53. Sultana, R., Ravagna, A., Mohmmad-Abdul, H., Calabrese, V., and Butterfield, D. A. (2005) *J Neurochem* **92**, 749-758
54. Luo, J., Chuang, T., Cheung, J., Quan, J., Tsai, J., Sullivan, C., Hector, R. F., Reed, M. J., Meszaros, K., King, S. R., Carlson, T. J., and Reaven, G. M. (1998) *Eur J Pharmacol* **346**, 77-79
55. Goodman, Y., Steiner, M. R., Steiner, S. M., and Mattson, M. P. (1994) *Brain Res* **654**, 171-176
56. Zhao, B. L., Li, X. J., He, R. G., Cheng, S. J., and Xin, W. J. (1989) *Cell Biophys* **14**, 175-185
57. Lim, G. P., Chu, T., Yang, F., Beech, W., Frautschy, S. A., and Cole, G. M. (2001) *J Neurosci* **21**, 8370-8377
58. Kim, D. S., Park, S. Y., and Kim, J. K. (2001) *Neurosci Lett* **303**, 57-61
59. Frautschy, S. A., Hu, W., Kim, P., Miller, S. A., Chu, T., Harris-White, M. E., and Cole, G. M. (2001) *Neurobiol Aging* **22**, 993-1005
60. Petersen, M., and Simmonds, M. S. (2003) *Phytochemistry* **62**, 121-125
61. Alkam, T., Nitta, A., Mizoguchi, H., Itoh, A., and Nabeshima, T. (2007) *Behav Brain Res* **180**, 139-145
62. Iuvone, T., De Filippis, D., Esposito, G., D'Amico, A., and Izzo, A. A. (2006) *J Pharmacol Exp Ther* **317**, 1143-1149

FOOTNOTES

This study was supported by Grants-in-Aid for Young Scientists (B) (K.O.), Scientific Research (A) (22240051) (H.N.), Scientific Research (B) (20390242) (M.Y.), and Knowledge Cluster Initiative [High-Tech Sensing and Knowledge Handling Technology (Brain Technology)] (M.Y.) from the Japanese Ministry of Education, Culture, Sports, Science and Technology, Japan, a grant to the Amyloidosis Research Committee from the Ministry of Health, Labour, and Welfare, Japan (K.O. and M.Y.), Novartis Foundation for Gerontological Research (K.O.), Alumni Association of Showa University School of Medicine (K.O.), JSPS Asian Core Program (H.N.), and NIH Grants AG027818 (D.B.T.) and AG027853 (M.G.Z.), and the Jim Easton Consortium for Alzheimer's Drug Discovery and Biomarkers at UCLA (D.B.T.). The authors thank Dr. Chunyu Wang (RPI) for providing models of the Aβ42 structures and Ms. Margaret Condron (UCLA) for technical assistance.

Abbreviations used are: Aβ, amyloid β-protein; ACSF, artificial cerebrospinal fluid; AD, Alzheimer's disease; AFM, atomic force microscopy; APP, amyloid precursor protein; αS, α-synuclein; APS, ammonium persulfate; CD, circular dichroism spectroscopy; Cur, curcumin; DMEM, Dulbecco's modified Eagle's medium; DTT, dithiothreitol; EM, electron microscopy; FA, ferulic acid; fAβ, Aβ fibrils; fEPSPs, field excitatory presynaptic potentials; GST, glutathione S-transferase; HEK, human embryonic kidney; HMW, high molecular weight; HSQC, heteronuclear single quantum coherence; LTD,

long-term depression; LTP, long-term potentiation; MTT, 3-[4,5-dimethylthiazol-2-yl]-2,5-diphenyltetrazolium bromide; Myr, myricetin; NDGA, nordihydroguaiaretic acid; NMR, nuclear magnetic resonance; PICUP, photo-induced cross-linking of unmodified proteins; RA, rosmarinic acid; RP-HPLC, reverse-phase high-performance liquid chromatography; Ru(bpy), tris(2,2'-bipyridyl)dichlororuthenium(II); SC, statistical coils; SDS, sodium dodecyl sulfate; SDS-PAGE, SDS-polyacrylamide gel electrophoresis; SEC, size-exclusion chromatography; STD, saturation transfer difference.

FIGURE LEGENDS

Fig. 1. Structures of myricetin (Myr), ferulic acid (FA), nordihydroguaiaretic acid (NDGA), curcumin (Cur), and rosmarinic acid (RA).

Fig. 2. Aβ and GST oligomerizations. PICUP, followed by SDS-PAGE and silver staining, was used to determine the effects of 10 and 100 μM Myr, FA, NDGA, Cur, or RA on oligomerization of Aβ40 (A), Aβ42 (B) or GST (C). "+" and "-" mean "with cross-linking" and "without cross-linking", respectively. The gel is representative of each of three independent experiments. AFM was performed on 25 μM un-cross-linked (D, E) and cross-linked (F-K) Aβ40 (D, F, H, J) and Aβ42 (E, G, I, K) with 0 (F, G), 100 μM Myr (H, I) or RA (J, K). Scale bars are 100 nm.

Fig. 3. Aβ secondary structure dynamics. CD was used to monitor peptide assembly. Aβ40 (A, C, E) or Aβ42 (B, D, F) were incubated at 37 °C for 6 days in 10 mM phosphate, pH 7.4, in buffer alone (A, B) or in the presence of 100 μM Myr (C, D) or RA (E, F). Spectra were acquired immediately at the start of the incubation period, d 0 (○), and after days 2 (▼), 3 (□), 5 (■), and 6 (◇). The spectra presented at each time are representative of those obtained during each of three independent experiments.

Fig. 4. Expanded HSQC spectra of uniformly ^{15}N-labeled Aβ42. The HSQC experiment detects ^{1}H that are directly bonded to the ^{15}N atoms, notably the backbone amide ^{1}H-^{15}N. The control spectrum of the Aβ42 alone (25 μM, pH 7.2, 5°C, **black crosspeaks**) is overlaid with the spectra of the Aβ42 (25 μM) containing RA (A) or Myr (B) both at 500 μM concentrations (**red crosspeaks**).

Fig. 5. Representative NMR/MD structural models of Aβ42 that show binding locations with the phenolic compounds. The molecular models of the Aβ42 that were obtained from a combined molecular dynamics and NMR approach (26). The **green-colored** ribbons depict the backbone atoms, with those regions showing chemical shift changes (indicative of binding to the phenolic compounds) are **red-colored**. Residues at the margins of the binding regions are labeled.

Fig. 6. Effects of myricetine (Myr) and rosmarinic acid (RA) on Aβ42-induced alterations of neuronal plasticity (LTP and LTD) in the hippocampal slices. (A and D) Typical fEPSP waveforms of pre- (black lines) and (A) post-tetanic or (D) post-low frequency conditioning (red lines) stimulation in each test group. Thirty waveforms were averaged. (B and E) Time course of %fEPSPs slope. A thick line indicates application of various test compounds. (B) An arrow indicates tetanus stimulation (100 Hz, 1 sec). (E) Dots above the thick line indicate low frequency conditioning stimulation (E, 1 Hz, 450 paired-pulse). (C and F) Comparison of % fEPSP slope among the five groups. Values are shown as the percentage of fEPSP slope relative to the baseline and presented as mean ± S.E. (n = 5). Differences reaching statistical significance are noted by line segments between samples, along with their associated *p-values*, where * signifies $p < 0.05$ and ** signifies $p<0.01$.

Fig. 1.

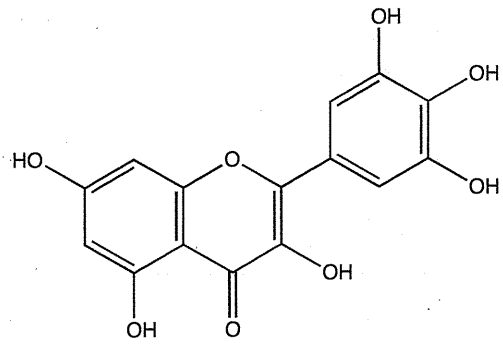

Myr

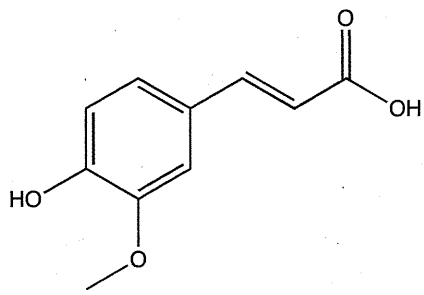

FA

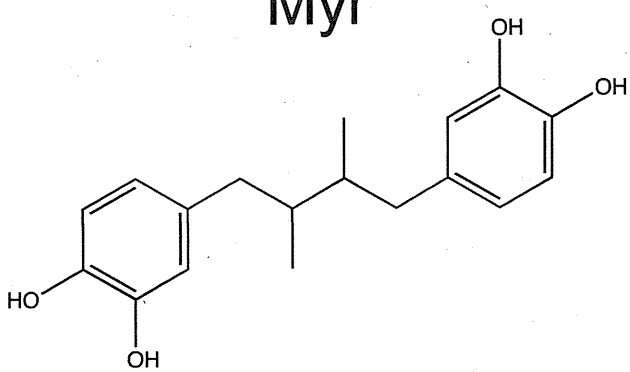

NDGA

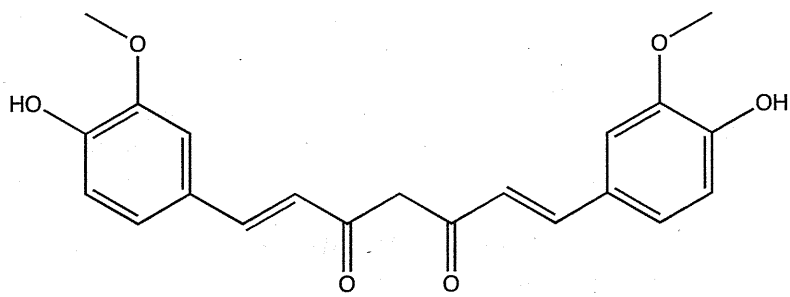

Cur

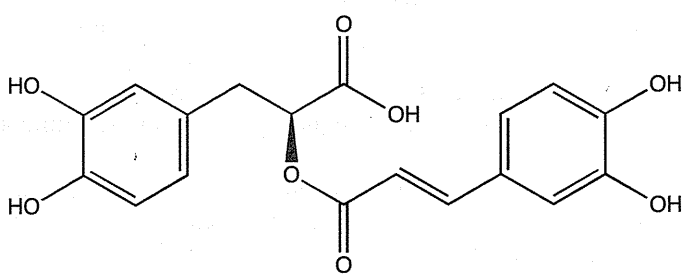

RA

Fig. 2.

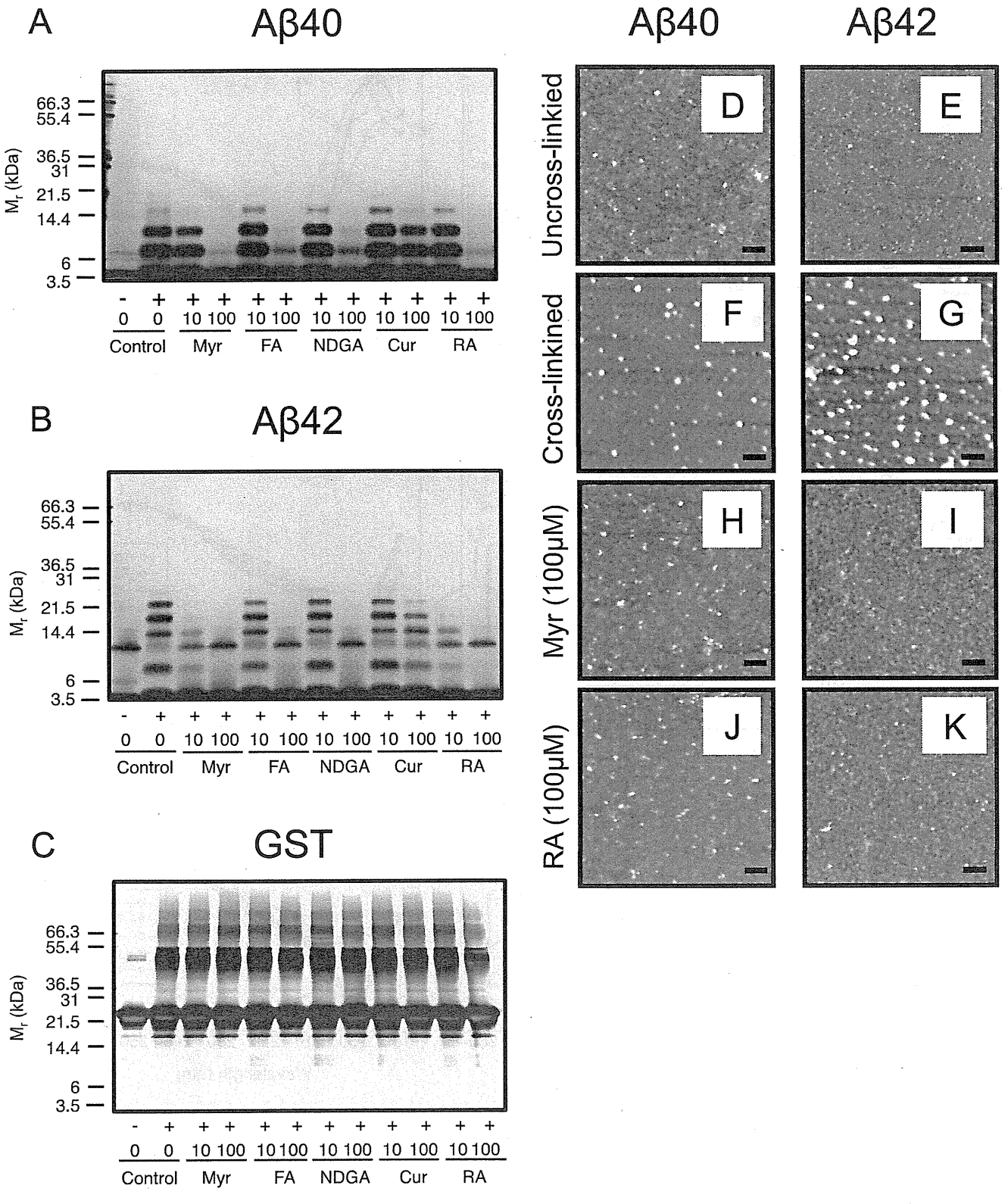
A
Aβ40
66.3
55.4
36.5
31
21.5
14.4
6
3.5
Mr (kDa)
- + + + + + + + + + + +
0 0 10 100 10 100 10 100 10 100 10 100
Control Myr FA NDGA Cur RA
B
Aβ42
66.3
55.4
36.5
31
21.5
14.4
6
3.5
Mr (kDa)
- + + + + + + + + + + +
0 0 10 100 10 100 10 100 10 100 10 100
Control Myr FA NDGA Cur RA
C
GST
66.3
55.4
36.5
31
21.5
14.4
6
3.5
Mr (kDa)
- + + + + + + + + + + +
0 0 10 100 10 100 10 100 10 100 10 100
Control Myr FA NDGA Cur RA
Aβ40
Aβ42
Uncross-linkied
Cross-linkined
Myr (100μM)
RA (100μM)
D
E
F
G
H
I
J
K

Fig. 3.

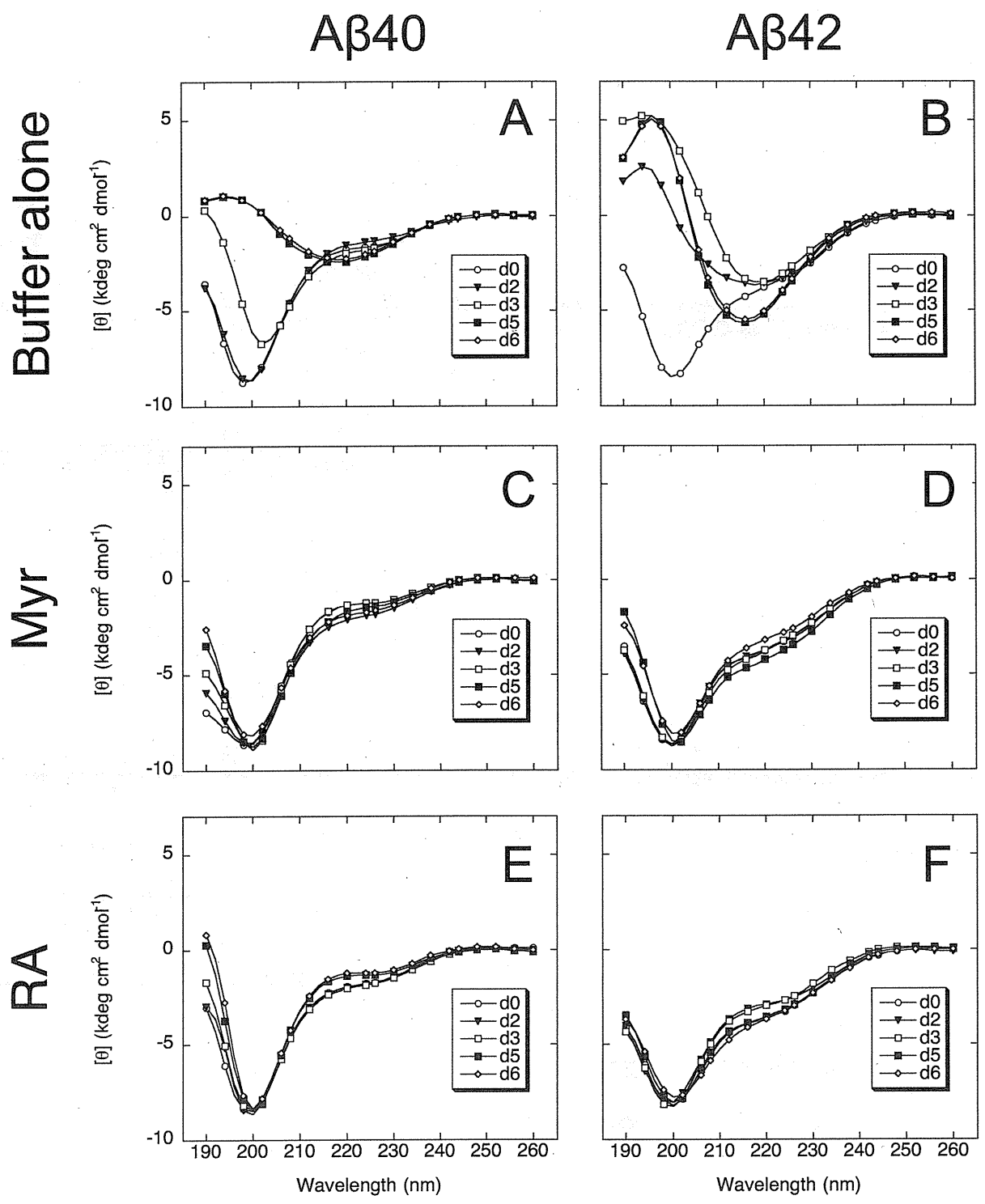
Aβ40
Aβ42
Buffer alone
Myr
RA
A
B
C
D
E
F
[θ] (kdeg cm² dmol⁻¹)
5
0
-5
-10
d0
d2
d3
d5
d6
190 200 210 220 230 240 250 260
Wavelength (nm)

Fig. 4.

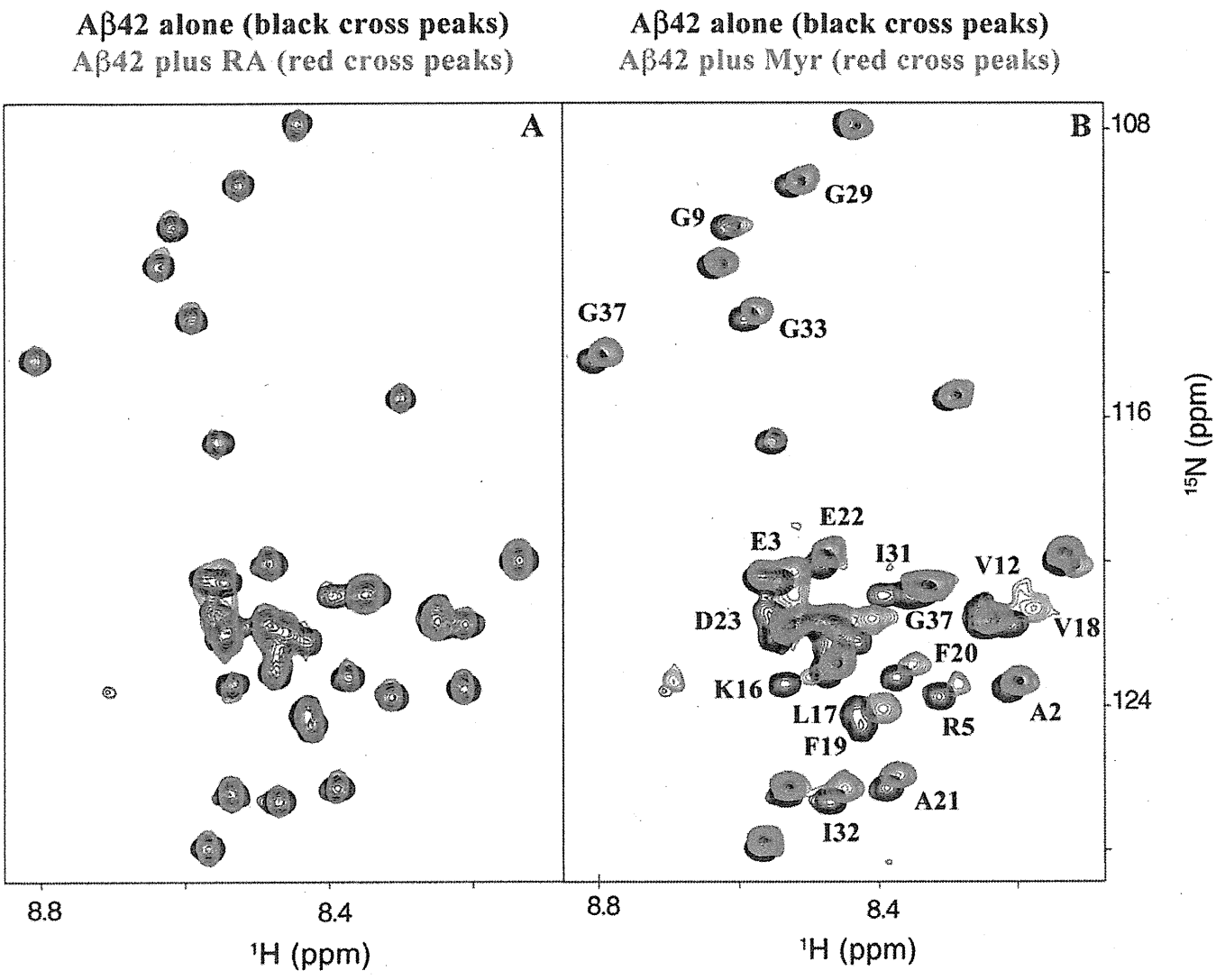
Aβ42 alone (black cross peaks)
Aβ42 plus RA (red cross peaks)
Aβ42 alone (black cross peaks)
Aβ42 plus Myr (red cross peaks)
A
B
G29
G9
G37
G33
E22
E3
I31
V12
D23
G37
V18
F20
K16
L17
R5
A2
F19
A21
I32
108
116
124
15N (ppm)
8.8
8.4
1H (ppm)
8.8
8.4
1H (ppm)

Fig. 5.

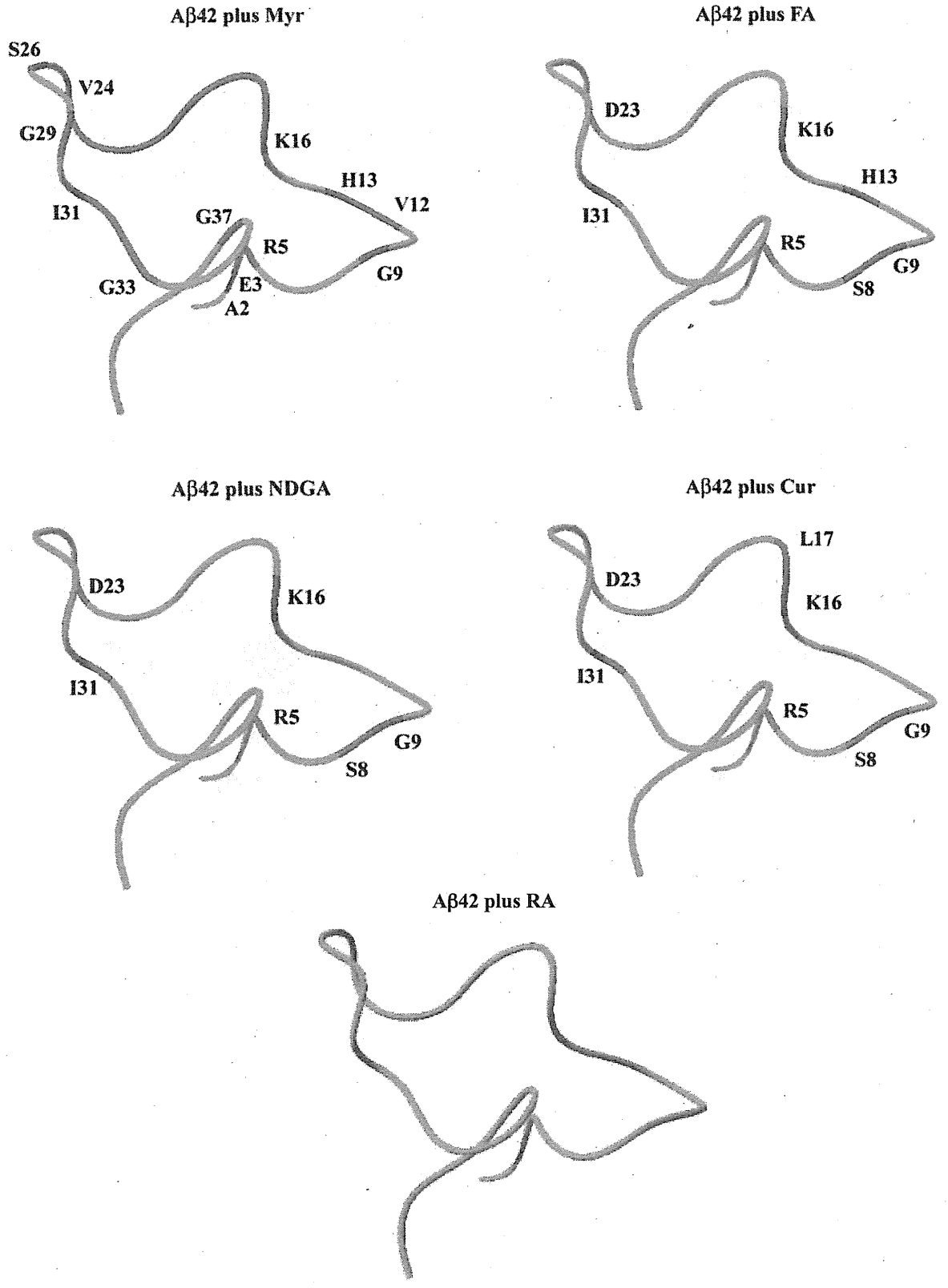
Aβ42 plus Myr
S26
V24
G29
K16
H13
V12
I31
G37
R5
G9
G33
E3
A2
Aβ42 plus FA
D23
K16
H13
I31
R5
G9
S8
Aβ42 plus NDGA
D23
K16
I31
R5
G9
S8
Aβ42 plus Cur
L17
D23
K16
I31
R5
G9
S8
Aβ42 plus RA

Fig. 6.

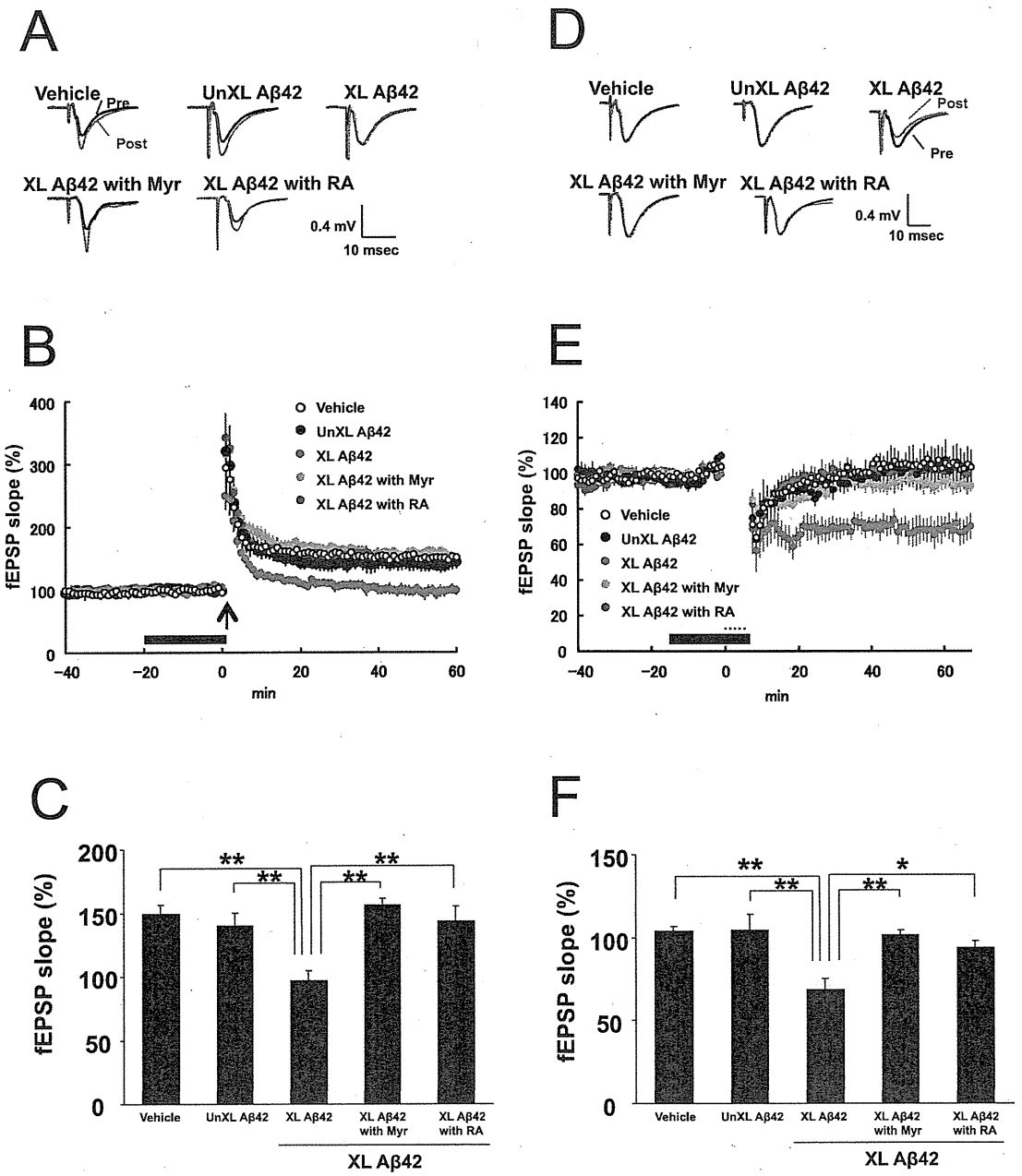
A
Vehicle
Pre
Post
UnXL Aβ42
XL Aβ42
XL Aβ42 with Myr
XL Aβ42 with RA
0.4 mV
10 msec
D
Vehicle
UnXL Aβ42
XL Aβ42
Post
Pre
XL Aβ42 with Myr
XL Aβ42 with RA
0.4 mV
10 msec
B
fEPSP slope (%)
Vehicle
UnXL Aβ42
XL Aβ42
XL Aβ42 with Myr
XL Aβ42 with RA
min
E
fEPSP slope (%)
Vehicle
UnXL Aβ42
XL Aβ42
XL Aβ42 with Myr
XL Aβ42 with RA
min
C
fEPSP slope (%)
Vehicle
UnXL Aβ42
XL Aβ42
XL Aβ42 with Myr
XL Aβ42 with RA
XL Aβ42
F
fEPSP slope (%)
Vehicle
UnXL Aβ42
XL Aβ42
XL Aβ42 with Myr
XL Aβ42 with RA
XL Aβ42

Aging Cell (2012) **11**, pp51–62 Doi: 10.1111/j.1474-9726.2011.00756.x

Adaptive responses to alloxan-induced mild oxidative stress ameliorate certain tauopathy phenotypes

Yuji Yoshiike,[1,2] Shunji Yamashita,[1] Tatsuya Mizoroki,[1] Sumihiro Maeda,[3] Miyuki Murayama,[1] Tetsuya Kimura,[1,4] Naruhiko Sahara,[5] Yoshiyuki Soeda[1] and Akihiko Takashima[1,4]

[1]Laboratory for Alzheimer's Disease, RIKEN Brain Science Institute, 2-1 Hirosawa, Wako-shi, Saitama 351-0198, Japan
[2]Alzheimer's Disease Project Team, The Research Institute, National Center for Geriatrics and Gerontology, 35 Gengo, Morioka, Obu, Aichi 474-8511, Japan
[3]Department of Neurology, Gladstone Institute of Neurological Disease, University of California, San Francisco, CA 94158, USA
[4]Center for Development of Advanced Medicine for Dementia, National Center for Geriatrics and Gerontology, 35 Gengo, Morioka, Obu, Aichi 474-8511, Japan
[5]Department of Neuroscience, Center for Translational Research in Neurodegenerative Disease, College of Medicine, University of Florida, Gainesville, FL 32610, USA

Summary

Oxidative stress is considered to promote aging and age-related disorders such as tauopathy. Although recent reports suggest that oxidative stress under certain conditions possesses anti-aging properties, no such conditions have been reported to ameliorate protein-misfolding diseases. Here, we used neuronal and murine models that overexpress human tau to demonstrate that mild oxidative stress generated by alloxan suppresses several phenotypes of tauopathy. Alloxan treatment reduced HSP90 levels and promoted proteasomal degradation of tau, c-Jun *N*-amino terminal kinase, and histone deacetylase (HDAC) 6. Moreover, reduced soluble tau (phosphorylated tau) levels suppressed the formation of insoluble tau in tau transgenic mice, while reduced HDAC6 levels contributed to microtubule stability by increasing tubulin acetylation. Age-dependent decreases in HDAC2 and phospho-tau levels correlated with spatial memory enhancement in alloxan-injected tau mice. These results suggest that mild oxidative stress, through adaptive stress responses, operates counteractively against some of the tauopathy phenotypes.

Key words: aging; Alzheimer's disease; memory; microtubule; oxidative stress; tau.

Introduction

The free radical theory of aging posits that aging and age-associated degenerative diseases may be attributed to the deleterious effects of free radicals on various cell components (Harman, 1956). Since the proposal of this theory by Harman in 1956, a great number of studies have supported but not proven this theory (Balaban *et al.*, 2005). Aerobic metabolism and the subsequent generation of reactive oxygen species (ROS) are widely accepted to cause aging. However, how aerobic metabolism and ROS generation are regulated and how oxidative stress and its targets might affect aging and age-related disorders remain unknown (Balaban *et al.*, 2005).

Macromolecular damage often found in misfolded proteins that accumulate with age is believed to cause aging and degenerative diseases (Kenyon, 2010). A prime candidate for causing age-related damage is ROS produced mainly during respiration in mitochondria, whose integrity has been shown to decline as a function of age (Sigenaga *et al.*, 1994). However, there are a growing number of exceptions to this theory. Some hypothesize that low levels of ROS might play a preventive role against aging, whereas high levels may play a causative role in aging (Gems & Partridge, 2008; Kenyon, 2010). For example, in *Caenorhabditis elegans*, low levels of juglone, which generates ROS, extend lifespan (Heidler *et al.*, 2010). In worms, glucose restriction extends lifespan by inducing mitochondrial respiration and by increasing oxidative stress (Schulz *et al.*, 2007). In yeast, caloric restriction also extends lifespan by inducing elevated levels of hydrogen peroxide, which activate superoxide dismutase (Mesquita *et al.*, 2010). Studies of long-lived species and transgenic (TG) mice with altered expression of antioxidants also suggest that oxidative damage is not directly correlated with lifespan (Van Remmen *et al.*, 2003). Thus, it is perhaps not only the oxidative stress but also the resistance mechanisms against oxidative stress that may determine the rate of aging (Perez *et al.*, 2009). Such adaptive stress responses might underlie hormesis, a phenomenon in which a compound that, at higher levels, produces deleterious effects, but at lower levels, produces beneficial effects (Mattson, 2008; Rattan & Demirovic, 2010). If low levels of ROS could delay aging processes under certain conditions, we surmised that there is also a hormetic condition that exists during oxidative stress that prevents protein misfolding and associated dysfunctions.

One of the normal functions of tau protein is to bind and stabilize microtubules in axons (Ballatore *et al.*, 2007). As a result of modifications such as phosphorylation, tau detaches from microtubules, which become destabilized (Mi & Johnson, 2006; Ballatore *et al.*, 2007). As a cytoskeletal component, microtubules, and importantly their stability, are considered to play substantial roles in neuronal function. Unless free soluble tau is degraded, it starts to aggregate, eventually becoming insoluble and forming intracellular neurofibrillary tangles (NFT), a pathological hallmark of tauopathies such as Alzheimer's disease (AD) (Yen *et al.*, 1995; Mi & Johnson, 2006; Ballatore *et al.*, 2007). The progression of cortical NFT formation is correlated with the degree of cognitive decline in AD (Braak & Braak, 1996). Therefore, tau aggregation, microtubule destabilization, and memory deficits are the critical phenotypes that result from tau misfolding and dysfunction.

Early studies examining the effects of oxidative stress on tau primarily focused on the phosphorylation states of tau and the kinases responsible for phosphorylating tau in acutely treated cells, because tau phosphorylation is considered to regulate the microtubule binding and stabilizing activity of tau (Zhu *et al.*, 2004; Mi & Johnson, 2006; Ballatore *et al.*, 2007). When cells are treated with acrolein, 4-hydroxy-2-nonenal (4-HNE), homocysteine, mercury, and Aβ peptide, tau phosphorylation increases (Zhu *et al.*, 2004). By contrast, when cells are treated with hydrogen peroxide (H_2O_2), ultraviolet light, menadione, or iron, tau phosphorylation decreases (Zhu *et al.*, 2004). Chronic application of oxidative stress in neuronal cells, *Drosophila*, and mouse models of tauopathy

Correspondence
Yuji Yoshiike, Alzheimer's Disease Project Team, The Research Institute, National Center for Geriatrics and Gerontology, 35 Gengo, Morioka, Obu, Aichi 474-8511, Japan. Tel.:/fax: +81 562 87 1278; e-mail: yyoshiik@ncgg.go.jp

Accepted for publication *2 October 2011*

through genetic manipulations induces neurodegeneration and tau accumulation (Zhu *et al.*, 2004; Dias-Santagata *et al.*, 2007; Kulic *et al.*, 2009). Here, we used a chemical named alloxan to investigate the acute effects of oxidative stress on cellular and mouse models of tauopathy.

Alloxan, which was originally synthesized by Wohler and Liebig, became of interest in diabetes research when Dunn and McLetchie reported its diabetogenic property in animals (Lenzen & Panten, 1988). Alloxan can generate ROS in a cyclic reaction along with its reduction product, dialuric acid (Lenzen & Panten, 1988; Lenzen, 2008). The reduction in alloxan to dialuric acid in cells typically requires the presence of the tripeptide glutathione (GSH) (Lenzen, 2008). Thus, in theory, oxidative stress can be induced by alloxan where a sufficient amount of GSH is available. The brains of alloxan-induced diabetic rats show not only high levels of blood glucose but also increased levels of oxidative stress markers, such as malondialdehyde (MDA) and thiobarbituric acid-reactive substances (TBARS) (Genet *et al.*, 2002; Siddiqui *et al.*, 2005). Taking advantage of accumulative information regarding its mode of action and dose responses *in vivo*, we decided to use alloxan for examining the role of oxidative stress in tau misfolding and related dysfunctions.

Mutations in the tau gene have been identified in familial forms of frontotemporal dementias that are characterized by NFT formation (Hutton, 2000). In the present study, we used a mouse neuronal cell line that stably expresses a mutant form of human tau (P301L) (Hatakeyama *et al.*, 2004) for elucidating the molecular impact of alloxan-generated oxidative stress on tau, tau phosphorylation, and stress-responsive proteins such as c-Jun *N*-amino terminal kinases (JNKs) and heat-shock proteins (HSPs). Experiments using H_2O_2, catalase, a HSP90 inhibitor, and a proteasomal inhibitor revealed that the degradation system, which adaptively responded to alloxan-generated ROS, was at least partially responsible for reducing tau and JNK. By injecting alloxan into TG mice expressing human mutant tau (P301L or R406W), we identified conditions that did not raise blood glucose levels but did reduce the formation of insoluble tau in cerebral cortex. In the case of alloxan-injected P301L TG mice, the reduction in insoluble tau was accompanied by a slight increase in the lipoperoxide MDA as well as a decrease in both soluble phosphorylated tau and HSP90. Proteasomes activated by alloxan degraded not only tau but also another HSP90 substrate, histone deacetylase (HDAC) 6, which in turn promoted the acetylation of its substrate, α-tubulin, *in vitro*. Corresponding changes in protein levels were also observed *in vivo*. Further analyses showed that HDAC2, another deacetylase of a different class, was also reduced by alloxan treatment and that age-dependent decreases in HDAC2 and phospho-tau levels were correlated with the enhancement of spatial memory in alloxan-injected P301L TG mice.

Results

Acute effects of alloxan on tau and stress-response proteins *in vitro*

Depending on the experimental conditions, oxidative stress has been known to increase or decrease the phosphorylation of tau in cells treated with ROS-generating compounds (Zhu *et al.*, 2004). We treated murine neuronal cells expressing P301L mutant human tau with alloxan in the presence of GSH. After 1 h of treatment, immunoreactivity against some tau phosphorylation sites increased, but after 5 h of treatment, immunoreactivity decreased and the respective bands shifted (Figs S1 and 1A). In other words, the intensity of phospho-tau band at higher molecular weight was lowered as total tau band migrated more, suggesting that tau was dephosphorylated by 5-h alloxan treatment. These alterations in phosphorylation pattern were mostly consistent with those observed from H_2O_2-treated cells (Fig. S1). Among the kinases known to phosphorylate tau, JNK and their phosphorylated and thus activated forms decreased with longer treatment periods (Figs S1 and 1A). These results were unexpected, as JNK is also known as stress-activated protein kinase (SAPK) (Zhu *et al.*, 2004; Dias-Santagata *et al.*, 2007). Phospho-JNK levels were increased in cells treated with H_2O_2 (Fig. S1). Indeed, redox reactions of alloxan in the presence of GSH showed that alloxan generated not only H_2O_2 but also other species that might have promoted the inactivation of JNK via an unknown mechanism.

Heat-shock proteins are proteins known to show increased expression during stress. Thus, we also examined the effect of alloxan on HSP expression: alloxan treatment for 5 h increased HSP90 and HSP70 levels (Fig. 1A). This suggests that these chaperones were expressed to prevent unstable proteins such as tau from aggregating. In the meantime, tau levels appeared to decrease as treatment time progressed. Increased polyubiquitination early on during treatment followed by its decrease indicates that the degradation system also responded in order to maintain cellular homeostasis (Fig. 1A).

After overnight treatment with alloxan, we observed that tau, HSP90, HSP40, and HSP27 levels decreased in a dose-dependent manner (Fig. S2A). These decreases were suppressed by adding catalase into the culture medium (Fig. S2B). Similar decreases in protein levels were observed in H_2O_2-treated cells (Fig. S2C). These results suggest that H_2O_2 generated from alloxan in the presence of GSH was responsible for reducing tau and HSP levels. Inhibiting HSP90 through inhibitors such as geldanamycin (GA) reduces the HSP90 substrates, including tau and JNK, in part through degradation (Dickey *et al.*, 2007; Luo *et al.*, 2007; Nieto-Miguel *et al.*, 2008; Novoselova *et al.*, 2008). Reductions in tau, JNK, and phospho-JNK levels were also observed in P301L tau-expressing cells treated with GA (Fig. 1B). The proteasome inhibitor lactacystin partially prevented the alloxan/GSH-induced reductions in tau and JNK levels but not that in HSP levels (Fig. 1C). These results suggest that alloxan-generated H_2O_2 promoted proteasomal degradation of HSP90 substrates, such as tau and JNK, conceivably via reduction in HSP90.

Low-dose alloxan–induced mild oxidative stress in the brain without inducing apparent diabetic symptoms

To test the impact of oxidative stress on the phenotypes associated with tau misfolding and dysfunction *in vivo*, we injected alloxan into TG mice that express human mutant (P301L) tau (Kimura *et al.*, 2010). A single intraperitoneal injection of alloxan at 100 mg kg^{-1} of body weight, on average, failed to significantly change either blood glucose concentration or body weight (Fig. 2A–D). Moreover, we found no statistically significant differences between the alloxan-treated group and vehicle (saline)-treated group, even after considering blood glucose concentration or body weight values from nontransgenic (NTG) and P301L mice together as a group. The latter indicates that diabetic complications did not develop, at least overall, in the experimental cohort as a result of alloxan treatment at the dosage of 100 mg kg^{-1}. Because significant increases in blood glucose levels (approximately 190 mg dL^{-1} in fasting mice) and decreases in body weights were observed in mice that had received higher doses of alloxan (400 mg kg^{-1} by i.p.), it is likely that the alloxan solution used in our experiments was potent enough to generate diabetes in mice (Fig. 2A,B). However, under the condition that clearly did not induce diabetic phenotypes in mice, we observed slight yet significant increases in MDA, a lipid peroxide marker that is normally elevated during oxidative stress in cerebral cortical homogenates from alloxan-treated mice (without separating by genotype) (Fig. 2E,F). Therefore, we assumed that alloxan caused oxidative stress, in the brains of these mice, even though its effect was mild.

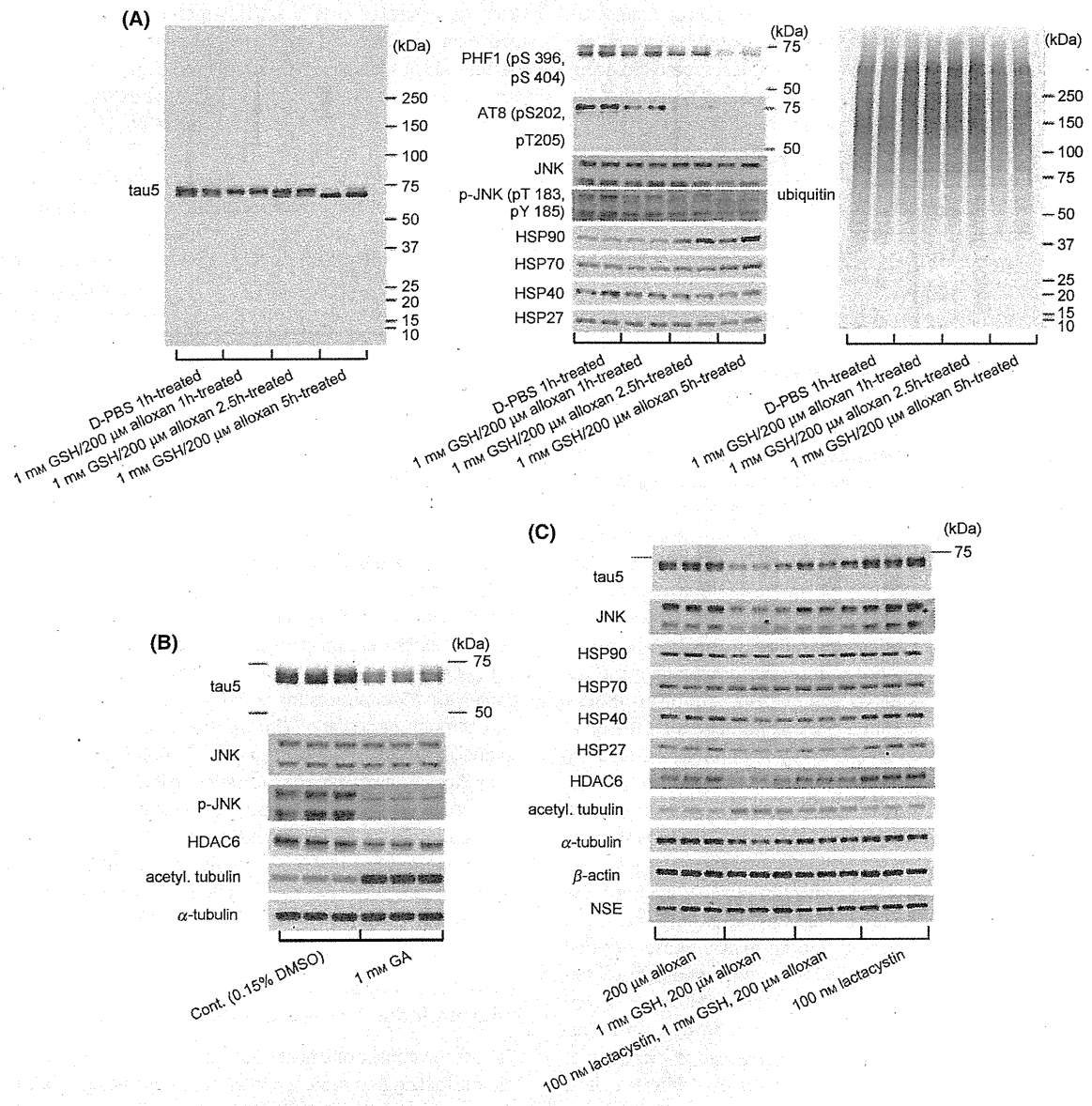

Fig. 1 Changes in protein levels as a result of alloxan treatment *in vitro*. (A) Alterations in the levels of tau, phospho-tau, c-Jun *N*-amino terminal kinase (JNK), phospho-JNK, heat-shock proteins (HSPs), and ubiquitin during alloxan treatment. Neuro2A cells stably expressing P301L tau were treated with alloxan in the presence of glutathione (GSH) for the indicated periods. After treatment, Tris-buffered saline (TBS)-soluble cell lysates derived from cell homogenates were analyzed by Western blotting. (B) Decreases in the levels of tau, JNK, phospho-JNK, and histone deacetylase (HDAC) 6 but increases in the levels of acetylated tubulin by HSP90 inhibition. Tau-expressing cells were treated with geldanamycin (GA), a HSP90 inhibitor, for 24 h, and mRIPA-soluble lysates were prepared and analyzed by Western blotting. (C) Partial blockade of alloxan-induced changes in tau, JNK, HDAC6, and acetylated tubulin protein levels by proteasomal inhibition. Tau-expressing cells were treated for 16 h with alloxan in the presence of GSH with or without lactacystin, a proteasomal inhibitor. TBS-soluble fractions derived from cell lysates were treated with the indicated antibodies except for anti-HDAC6, which was used to treat 2% SDS-soluble fractions containing more nuclear extracts.

Malondialdehyde levels in alloxan-treated mice varied according to the age of the mice (Fig. S3A). Because oxidative stress increases with age (Balaban *et al.*, 2005; Cocheme *et al.*, 2011), it is tempting to speculate that ROS accumulation owing to aging and ROS generated from alloxan were combined, resulting in higher MDA levels in older mice.

Suppression of tau insolubilization in mutant tau transgenic mice injected with alloxan

Next, we examined the levels of tau protein and stress-responsive proteins in cortical homogenates derived from saline- and alloxan-injected P301L mice (Fig. 3). Quantification of immunoreactivity showed that HSP90 immunoreactivity was inversely proportional to MDA level (Fig. 4A), indicating that HSP90 levels decrease as lipid peroxide levels, and thus oxidative stress, increase. Consistent with the cell culture results, alloxan injections significantly reduced HSP90 levels in P301L mouse brain (Fig. 4B). The HSP90 decrease was directly associated not only with a decrease in sarcosyl-insoluble tau but also with a decrease in JNK (Fig. 4C,D), as observed in the cell culture experiments, which showed that HSP90 substrates, including tau and JNK, were degraded upon oxidative stress (Fig. 1). In addition, the levels of several phospho-tau proteins (tau-phosphorylated at different epitopes) were decreased, as was

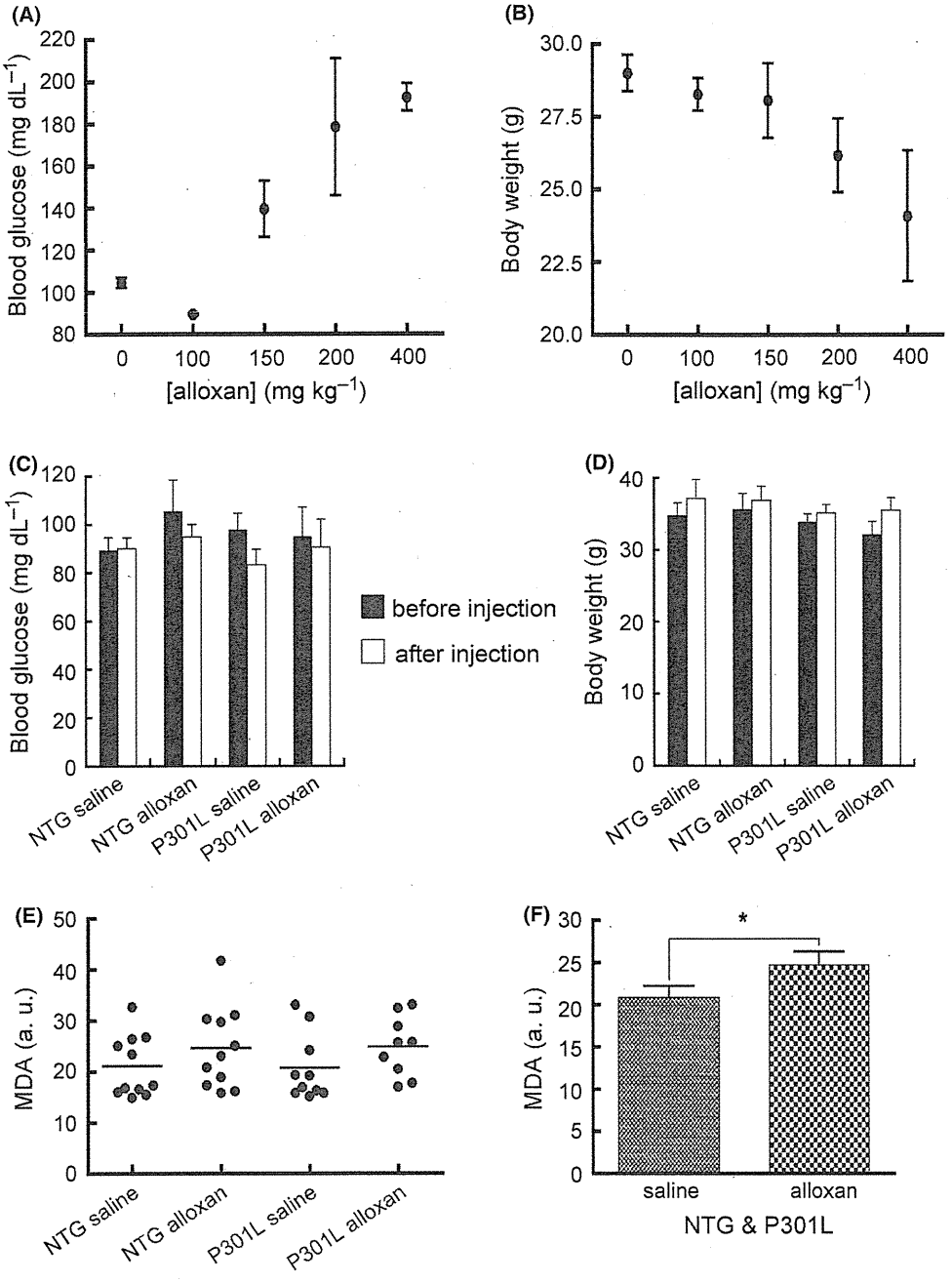

Fig. 2 Low-dose alloxan injection induced no significant changes in blood glucose and body weight but slightly induced oxidative stress in mouse brain. (A) Dose-dependent increase in blood glucose concentrations by alloxan injections in C57BL/6J mice (P = 0.0417, Friedman). (B) Dose-dependent decrease in body weight by alloxan injections in C57BL/6J mice (P = 0.0417, Friedman). (C) Blood glucose concentrations in nontransgenic (NTG) and P301L transgenic (TG) mice before and after injections of alloxan or saline vehicle. No significant difference between groups after treatment (P = 0.3750, Friedman) or by treatment after combining NTG and TG (P = 0.3486) was detected. (D) Simultaneous measurement of body weight. No significant difference between groups was detected after treatment (P = 0.7741, Friedman) or by treatment after combining NTG and TG (P = 0.7842). (E) Variation in malondialdehyde (MDA) values within each group. No significant difference was detected between groups (P = 0.1623, Friedman). (F) Significantly higher MDA levels in alloxan-treated mice than in saline-treated mice when MDA level values of NTG and P301L mice were considered together as a group (P = 0.0461).

phospho-JNK1 (i.e., activated JNK1), in the alloxan-treated P301L mice (Fig. 4E). Although this decrease at each phosphorylation site was not significant, the overall reduction in phospho-tau proteins was statistically significant when comparing the alloxan-treated group to the saline-treated group (Fig. 4F). In alloxan-injected P301L mice, decreased soluble phospho-tau levels were correlated with a significant decrease in insoluble tau levels (Fig. 4G,H). An inverse association also existed between MDA levels and insoluble tau levels (Fig. S3B), suggesting that alloxan-generated ROS may play a role in reducing insoluble tau levels (Fig. 4H). These results together with the cell culture results suggest that the reduction in HSP90 levels that occurred in response to alloxan-generated oxidative stress induced the degradation of HSP90 substrates – tau,

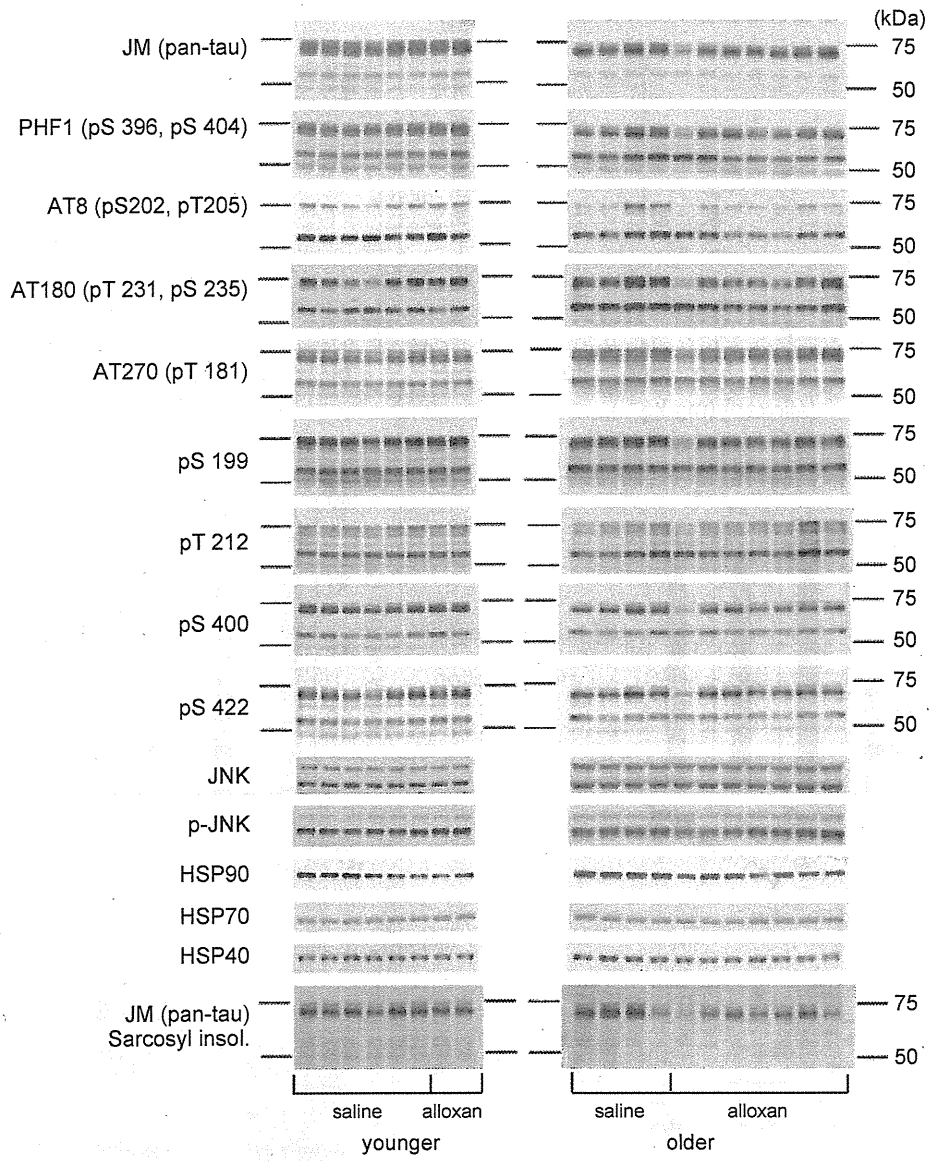

Fig. 3 Western blot analyses of Tris-buffered saline-soluble and sarcosyl-insoluble fractions derived from the brains of P301L mice treated with either saline or alloxan. Note that clearer differences were observed between saline- and alloxan-treated groups in relatively older cohorts. These age-dependent variations made treatment effects less substantial in some of the biochemical and functional parameters but allowed us to find significant correlations between those parameters.

phospho-tau, and JNK. This degradation perhaps suppressed the formation of insoluble tau in P301L mice as well.

Mouse models of type 1 diabetes have been reported to show increased phosphorylations of tau (Clodfelder-Miller *et al.*, 2006). We next injected a diabetogenic dose of alloxan into NTG and P301L TG mice for confirming such a phenomenon in alloxan paradigm and for examining effects on tau homeostasis and aggregation. A single intraperitoneal injection of alloxan at 300 mg kg^{-1} of body weight resulted in 73.3% lethality in mice within 10 days after injection. The excessive increase in blood glucose levels and the drop in body weights of survived mice suggested that these mice have diabetes (Fig. S4A,B). Murine cerebral cortices were homogenized, and the resulting fractions were analyzed biochemically by the same procedure as in the case of low-dose alloxan experiments. PHF1 and AT8-positive tau were increased in alloxan-injected NTG mice (Fig. S4C), confirming the effects of diabetes induced by other methods such as streptozotocin injection (Clodfelder-Miller *et al.*, 2006). Surprisingly, no such increases in phospho-tau levels were observed in alloxan-injected P301L mice in comparison with saline-injected P301L mice. Accordingly, insoluble tau levels also showed no difference between saline- and alloxan-injected P301L mice. In search of molecular factors rationalizing these phenomena, we found two factors that affected TG mice but not NTG mice as a result of alloxan injection. GSK3β level was slightly but significantly reduced in the alloxan-injected P301L mice (Fig. S4D). Reduction in this tau protein kinase is a potential reason for the suppression of the increase in phospho-tau levels. In addition, HSP90 was even more clearly reduced in P301L mice but not in NTG mice by the alloxan injection (Fig. S4C,D). Considering the difference between NTG and P301L, it seems logical to suspect that the suppression of phospho-tau enhancement in P301L mice is related to the overexpression of mutant tau. Therefore, we extrapolated that alloxan-induced oxidative stress triggered adaptive stress responses such as HSP90 reduction only where the unfolded protein, tau in this case, was overloaded. This